

A cocktail of SARS-CoV-2 S stem helix domain and receptor binding domain human monoclonal antibodies prevents the emergence of viral escape mutants

Yao Ma,¹ Chengjin Ye,¹ Michael S. Piepenbrink,² Sara H. Mahmoud,^{1,3} Anastasija Cupic,^{4,5} Esteban Castro,¹ Nathaniel Jackson,¹ Mahmoud Bayoumi,^{1,6} Alvaro S. Padron,¹ Adolfo García-Sastre,^{5,7,8,9,10,11} Gregory C. Ippolito,¹ Mark R. Walter,¹² James J. Kobie,² Luis Martinez-Sobrido¹

AUTHOR AFFILIATIONS See affiliation list on p. 12.

ABSTRACT Neutralizing antibodies (NAbs) targeting the spike (S) glycoprotein remain a crucial therapeutic strategy against severe acute respiratory syndrome coronavirus 2 (SARS-CoV-2). However, emerging viral variants have escaped all Food and Drug Administration (FDA)-approved NAb treatments, underscoring the urgent need for effective therapeutic alternatives. Using a nanoluciferase (Nluc)-expressing attenuated recombinant SARS-CoV-2 lacking the open reading frames (ORFs) 3a and 7b (Δ 3a7b-Nluc), we characterized resistance profiles of two broadly protective NAbs targeting the S receptor binding domain (RBD) in S1 (1301B7) and the stem helix domain (SH) in S2 (1249A8). Serial passaging of Δ 3a7b-Nluc under selective pressure identified a 1301B7 antibody-resistant mutant (ARM-B7) harboring an RBD mutation (S371F) that conferred resistance to 1301B7 and other RBD-directed NAbs (casirivimab, SC27, and sotrovimab). In contrast, no ARM emerged under treatment with 1249A8 or an antibody cocktail of 1301B7 (RBD) + 1249A8 (SH). These findings demonstrate that escape mutations in S2 SH are not easily tolerated by the virus compared with S1 RBD, and that a NAbs cocktail therapy targeting the SARS-CoV-2 S1 RBD and S2 SH offers the most effective strategy to prevent the emergence of escape mutations. Together, our findings provide critical insights into developing next-generation resistance-evading NAb therapies against SARS-CoV-2, and potentially other coronaviruses, and demonstrate the value of using our attenuated viral platforms for the safe identification of ARM without the potential biosafety concerns of doing these experiments using wild-type (WT) forms of SARS-CoV-2.

IMPORTANCE The clinical efficacy of early SARS-CoV-2 NAbs has been challenged by the emergence of escape viral variants, highlighting an urgent need to anticipate resistance. Using a luminescent attenuated SARS-CoV-2 platform, we profiled resistant mutations against two broadly protective SARS-CoV-2 NAbs. Passage of Δ 3a7b-Nluc in the presence of a NAb targeting the RBD S1 domain (1301B7) readily selected for an ARM, whereas passage in the presence of an SH S2 domain NAb (1249A8) did not. Notably, a cocktail of 1301B7 and 1249A8 created a high barrier of selecting SARS-CoV-2 ARM, preventing the emergence of resistant variants. We identified an S371F mutation in the S1 RBD of ARM-B7 that confers resistance to 1301B7 and other S1 RBD-targeting NAbs. These results highlight the importance of combination therapies targeting both variable RBD S1 and conserved SH S2 domain for the efficient treatment of SARS-CoV-2 and to prevent the emergence of NAb-induced escape mutations.

KEYWORDS COVID-19, SARS-CoV-2, attenuated virus, antibody-resistance mutant, spike protein

Editor Harold Marcotte, Karolinska Institutet, Stockholm, Sweden

Address correspondence to Mark R. Walter, walter@uab.edu, James J. Kobie, jkkobie@uabmc.edu, or Luis Martinez-Sobrido, lmartinez@txbiomed.org.

The A.G.-S. laboratory has received research support from Avimex, Dynavax, Pharmamar, 7Hills Pharma, ImmunityBio, and Accurius, outside of the reported work. A.G.-S. has consulting agreements for the following companies involving cash and/or stock: Castlevax, Amovir, Vivaldi Biosciences, Contrafect, 7Hills Pharma, Avimex, Pagoda, Accurius, Esperovax, Applied Biological Laboratories, Pharmamar, CureLab Oncology, CureLab Veterinary, Synairgen, Paratus, Pfizer, Virofend, and Prosetta, outside of the reported work. A.G.-S. has been an invited speaker in meeting events organized by Seqirus, Janssen, Abbott, AstraZeneca, and Novavax. A.G.-S. is an inventor on patents and patent applications on the use of antivirals and vaccines for the treatment and prevention of virus infections and cancer owned by the Icahn School of Medicine at Mount Sinai, New York, outside of the reported work. M.S.P., M.R.W., L.M.-S., and J.J.K. are co-inventors on patents that include claims related to the mAbs described. None of the other authors report any conflict of interest.

Received 2 January 2026

Accepted 28 February 2026

Published 5 May 2026

Copyright © 2026 Ma et al. This is an open-access article distributed under the terms of the [Creative Commons Attribution 4.0 International license](https://creativecommons.org/licenses/by/4.0/).

Over the past 5 years, coronavirus disease 2019 (COVID-19) has been responsible for over 700 million infections and approximately 7 million deaths (1). Notably, severe acute respiratory syndrome coronavirus 2 (SARS-CoV-2), the virus responsible for the COVID-19 pandemic, continues to evolve (2–5). Vaccines developed against the original SARS-CoV-2 strain no longer protect against emerging viral variants (6–10). Similarly, monoclonal neutralizing antibodies (NAbs) granted emergency use authorization (EUA) in the United States (US) rapidly lost effectiveness against newly emerging SARS-CoV-2 variants, and clinical use authorization of NAbs was revoked in early 2023 (11–13). The emergence of SARS-CoV-2 mutant strains necessitated the continuous updating of vaccines. Therefore, how to maximize protection against the emergence of new variants and suppress the emergence of escape mutations induced after vaccination have become an issue for the treatment of SARS-CoV-2 infections.

The receptor-binding domain (RBD) of SARS-CoV-2 spike (S) glycoprotein S1 region is a critical target for NAbs due to its role in mediating viral entry via binding to the angiotensin-converting enzyme 2 (ACE2) receptor (14, 15). However, the accumulation of mutations in the RBD of S1 across emerging variants has rendered many NAb therapies ineffective (11–13). A human monoclonal NAb, 1301B7, was isolated from a convalescent individual following Omicron infection in spring of 2023 using RBD-ACE2 fusion protein-based B cell isolation to enrich for antibodies targeting conserved ACE2-binding epitopes (16). 1301B7 exhibits broad and potent neutralization against SARS-CoV-2 original WA.1 strain as well as multiple viral variants, including Omicron subvariants BA.5, XBB.1.5, and JN.1, due to its unique binding mechanism involving the VH1-69 heavy chain and a long CDRH3 loop that engages conserved RBD S1 residues while tolerating mutations at positions like 417 and 456 residues (16).

Compared to the highly variable S1, the S2 stem domain demonstrates significant evolutionary conservation across β -coronaviruses, positioning it as a critical target for universal coronavirus antibodies and vaccines development (17–21). 1249A8 is a human NAb targeting the conserved membrane-proximal S2 stem helix (SH) region, thereby circumventing the immune evasion mechanisms associated with the highly variable SARS-CoV-2 RBD S1, making it an important candidate for universal coronavirus therapeutics (22–24). By disrupting the secondary structure and refolding events required for coronavirus post-fusion S to initiate membrane fusion and ultimately infection, 1249A8 demonstrates broad neutralizing activity against multiple β -coronaviruses, including SARS-CoV-2, SARS-CoV, and MERS-CoV (22, 23). For this reason, 1249A8 exhibits potent neutralizing activity against SARS-CoV-2 and SARS-CoV in different animal models, demonstrating its universal β -coronavirus therapeutic potential (23).

The Δ 3a7b-Nluc platform is a luminescent, attenuated recombinant SARS-CoV-2 engineered to enable the safe and efficient identification of antiviral-resistant mutants while circumventing the biosafety risks associated with using wild-type (WT) virus (25, 26). This system combines two key features: first, deletion of open reading frame (ORF) 3a and 7b accessory proteins of SARS-CoV-2 USA-WA1/2020 strain (GenBank accession no. [MN985325](#)), which attenuates viral pathogenicity while preserving replication (25, 27, 28); and second, expression of Nluc for real-time, high-throughput easy quantification of viral infection dynamics (26). The system maintains susceptibility to clinically relevant Food and Drug Administration (FDA)-approved or investigational antiviral compounds while being attenuated, allowing drug resistance profiling without the biosafety concerns associated with using WT SARS-CoV-2.

In this study, we employed Δ 3a7b-Nluc to evaluate the emergence of antibody-resistant mutants (ARMs) through serial passaging under increasing concentrations of NAbs. The study focused on two broad NAbs: 1301B7 (targeting RBD S1) and 1249A8 (targeting SH S2) alone or in combination. Following seven rounds of selection of Δ 3a7b-Nluc with 1301B7, we isolated an antibody-resistant mutant (ARM-B7) exhibiting significantly reduced neutralization (NT_{50} increase > 360-fold). Next-generation sequencing (NGS) identified a dominant non-synonymous RBD S1 mutation (S371F) in ARM-B7. In contrast, parallel passaging of Δ 3a7b-Nluc in the presence of 1249A8 failed to yield viruses with

significant resistance, suggesting a low tolerance for mutations in the S2 SH region. Additionally, serial passage of $\Delta 3a7b$ -Nluc in the presence of both NAb (1301B7 + 1249A8) avoided resistance development, without significant change in viral neutralization after seven viral passages. These findings demonstrate that S2 SH-targeting NAb like 1249A8 exhibit superior resistance profiles compared to S1 RBD-targeting NAb like 1301B7, and that a cocktail of S2 SH and S1 RBD targeting NAb (1249A8 + 1301B7) can efficiently prevent the emergence of ARMs. Furthermore, we identified the S371F mutation as an important mutation to reduce the neutralizing activity of S1 RBD-targeting NAb. We also demonstrate that our attenuated recombinant SARS-CoV-2 expressing Nluc ($\Delta 3a7b$ -Nluc) platform represents a safe option to identify ARMs from monoclonal NAb, or potentially sera preparations, to avoid biosafety concerns of using WT SARS-CoV-2.

RESULTS

Conservation of antibody-binding epitopes

Previous studies from our groups have shown that NAb 1301B7 and 1249A8 target distinct structural regions within the SARS-CoV-2 S protein (Fig. 1A) (16, 22). 1301B7 binds a conformational epitope mainly made of 11 amino acids within the S1 RBD (16) (Fig. 1A), while 1249A8 recognizes a linear epitope spanning 12 amino acid residues in the membrane-proximal S2 SH region (Fig. 1A) (22). Conservation analysis across major SARS-CoV-2 variants revealed that four residues within the 1301B7 epitope (positions 421, 453, 489, and 494) remain invariant, while the remaining seven amino acids exhibit variant-specific substitutions, with JN.1 accumulating the highest mutational burden (six altered residues) (Table 1). In contrast, the epitope of 1249A8 shows complete conservation across all major SARS-CoV-2 variants without observed

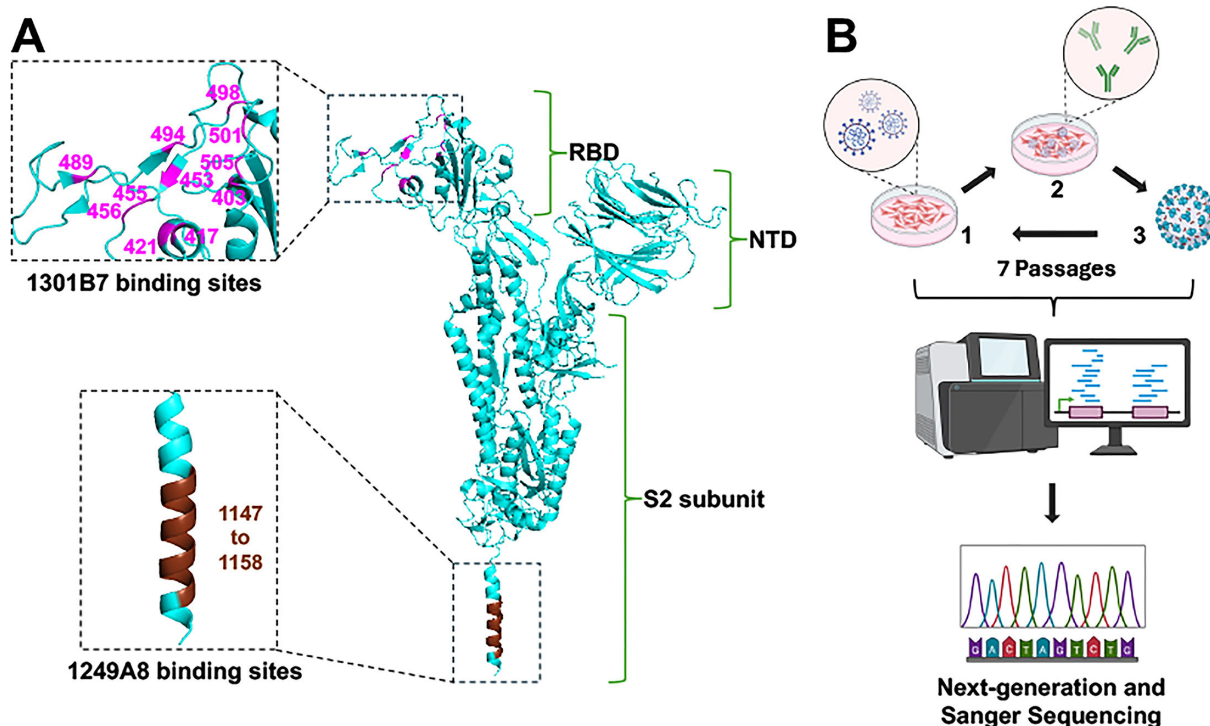


FIG 1 Neutralizing antibody (NAB) binding sites and selection of antibody-resistant mutants (ARMs). (A) Location of binding sites in the SARS-CoV-2 S protein (cyan, PDBID:6XR8) for 1301B7 (magenta), which targets the S1 RBD, and 1249A8 (brown), which targets the S2 SH. (B) Schematic of ARM selection: the attenuated recombinant SARS-CoV-2 expressing nanoluciferase ($\Delta 3a7b$ -Nluc) was serially passaged in Vero-AT cells under increasing concentrations of NAb. RNA from the Passage 7 viral populations was subjected to next-generation sequencing (NGS) and Sanger sequencing to identify resistance-associated mutations.

TABLE 1 Conservation of 1301B7 and 1249A8 binding sites in SARS-CoV-2 variants^a

	WA.1	B.1.1.7	B.1.351	P.1	AY.4	BA.1	BA.2	BA.5	EG.5	XBB.1.5	JN.1
1301B7	R403										R403K
	K417		K417N	K417T		K417N	K417N	K417N	K417N	K417N	K417N
	Y421										
	Y453										
	L455										L455S
	F456								F456L		
	Y489										
	S494										
	Q498					Q498R	Q498R	Q498R	Q498R	Q498R	Q498R
	N501	N501Y	N501Y	N501Y		N501Y	N501Y	N501Y	N501Y	N501Y	N501Y
Y505					Y505H	Y505H	Y505H	Y505H	Y505H	Y505H	
1249A8	S1147										
	F1148										
	K1149										
	E1150										
	E1151										
	L1152										
	D1153										
	K1154										
	Y1155										
	F1156										
	K1157										
	N1158										

^aThe information comes from outbreak.info (available online: <https://outbreak.info/>).

mutations, highlighting its structural stability and potential as a resilient therapeutic target (Table 1). 1301B7 (16) and 1249A8 (23) individual neutralizing activity against SARS-CoV-2 was previously described. Their potential synergistic neutralizing activity was evaluated using a checkerboard dilution assay (Fig. S1). Serial dilutions of each NAb expressed as multiples of its individual 50% neutralization titer (NT₅₀) were combined and tested for their capacity to neutralize Δ3a7b-Nluc (Fig. S1). The results demonstrate that the neutralization potency of 1301B7 was not compromised by co-incubation with 1249A8, and similarly, 1249A8 activity was independent of 1301B7 concentration. Specifically, at fixed concentrations of 1249A8, increasing the amount of 1301B7 reduced viral spot counts. Likewise, at fixed concentrations of 1301B7, increasing concentrations of 1249A8 also decreased viral spots. This absence of competitive inhibition implies that the two antibodies bind to independent epitopes. Notably, we observed a synergistic neutralizing activity when both NAbS were combined (Fig. S1).

Isolation of ARMs

To investigate the development of antibody resistance, Δ3a7b-Nluc was serially passaged in Vero-AT cells under increasing concentrations of 1301B7, 1249A8, or a cocktail of 1301B7 + 1249A8 (Fig. 1B and 2A). Following seven serial passages, a variant with significant resistance to 1301B7 (ARM-B7) was isolated (Fig. 2B). In contrast, parallel serial passage of Δ3a7b-Nluc under increasing concentrations of 1249A8 did not yield viruses with significant enhanced resistance (ARM-A8). From the fourth passage onwards, we did not observe increased viral resistance to 1249A8, indicating a low tolerance for mutations in the S2 SH region targeted by 1249A8 (Fig. 2B). Notably, the combination of both neutralizing antibodies (1301B7 + 1249A8) also suppressed the emergence of ARM-B7 + A8-resistant viruses, and we did not observe increased viral resistance to 1301B7 + 1249A8 after the third passage (Fig. 2B).

To quantitatively assess the neutralization resistance of the ARMs, we performed plaque reduction neutralization tests (PRNT) to determine the NT₅₀. ARM-B7 mutant

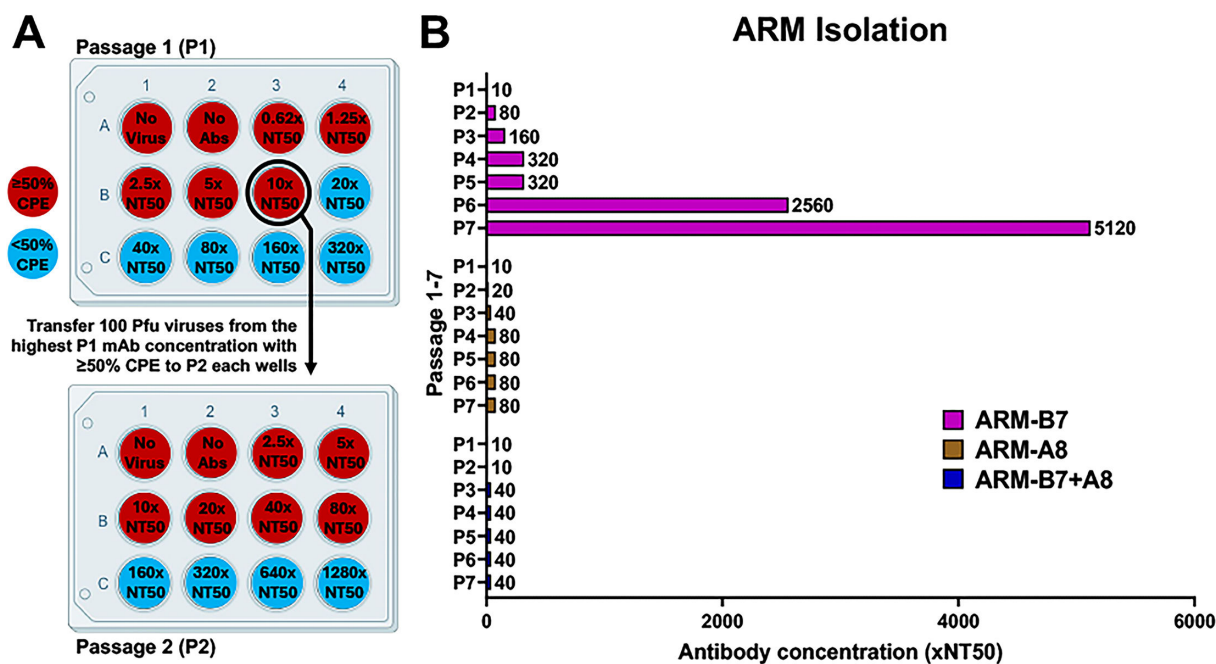


FIG 2 Isolation of ARMs. (A) Vero-AT cell monolayers were infected with $\Delta 3a7b$ -Nluc (100–200 PFU/well) and treated with escalating concentrations of 1301B7 ($NT_{50} = 5.66$ ng/mL) and 1249A8 ($NT_{50} = 2.09$ μ g/mL) alone or their combination. After 72 h of infection, cell culture supernatants from wells showing $\geq 50\%$ cytopathic effect (CPE) at the highest NAb concentration were harvested to initiate the next passage. Viral load was quantified by Nluc activity. (B) Passaging result of ARMs isolation is shown as multiples of the antibody NT_{50} concentration.

exhibited a profound (~ 360 -fold increase) resistance to 1301B7 ($NT_{50} = 2.04$ μ g/mL) compared to the parental $\Delta 3a7b$ -Nluc virus ($NT_{50} = 5.66$ ng/mL) (Fig. 3A and C). In contrast, ARM-A8 ($NT_{50} = 7.93$ ng/mL) and ARM-B7 + A8 ($NT_{50} = 8.17$ ng/mL) mutants remain similarly neutralized by 1301B7, with less than twofold increase in NT_{50} (Fig. 3A and C). Importantly, ARM-B7, ARM-A8, and ARM-B7 + A8 mutants displayed only a modest (less than fivefold) increase in resistance to 1249A8 compared to $\Delta 3a7b$ -Nluc (Fig. 3B and C). Specifically, the NT_{50} values for ARM-B7, ARM-A8, and ARM-B7+A8 against 1249A8 were 5.51, 9.55, and 4.20 μ g/mL, respectively. These values are comparable to 2.09 μ g/mL for the original $\Delta 3a7b$ -Nluc.

Identification of amino acid mutations responsible for ARMs

To identify the genetic determinants of viral resistance, we conducted next-generation sequencing (NGS) on viral RNA extracted from infected Vero-AT cells, focusing on variants with a frequency $>30\%$ (Fig. 4A). ARM-B7 (selected with 1301B7) contained three mutations in NSP1 (D139Y), NSP13 (V45A), and S (S371F). ARM-A8 (selected with 1249A8) harbored also three mutations in NSP3 (T847I), NSP16 (A34V), and S (T299I). ARM-B7 + A8 mutant (selected with the 1301B7 and 1249A8 cocktail) contained four mutations in NSP1 (D139Y), NSP10 (C41W), NSP13 (V45A), and NSP14 (M58I). No mutations were identified in the S glycoprotein of ARM-B7 + A8 after serial passages. After seven consecutive passages, the control group in the absence of antibody (P7 PBS) accumulated four mutations in NSP6 (A136V), NSP12 (M734R), E protein (T30I), and ORF8 (S84L) (Fig. 4A). Perhaps, this is because the virus grows to higher titers in PBS without antibody pressure and, therefore, generates more diversity. Some mutations could be tissue adaptation. Some mutations could be just neutral, and both are likely to accumulate faster when there is more replication.

Since both NAb target the S protein, we hypothesized that the mutations S371F in ARM-B7 and T299I in ARM-A8 were primarily responsible for the increased neutralizing resistance observed. To further validate our initial NGS results, we conducted Sanger

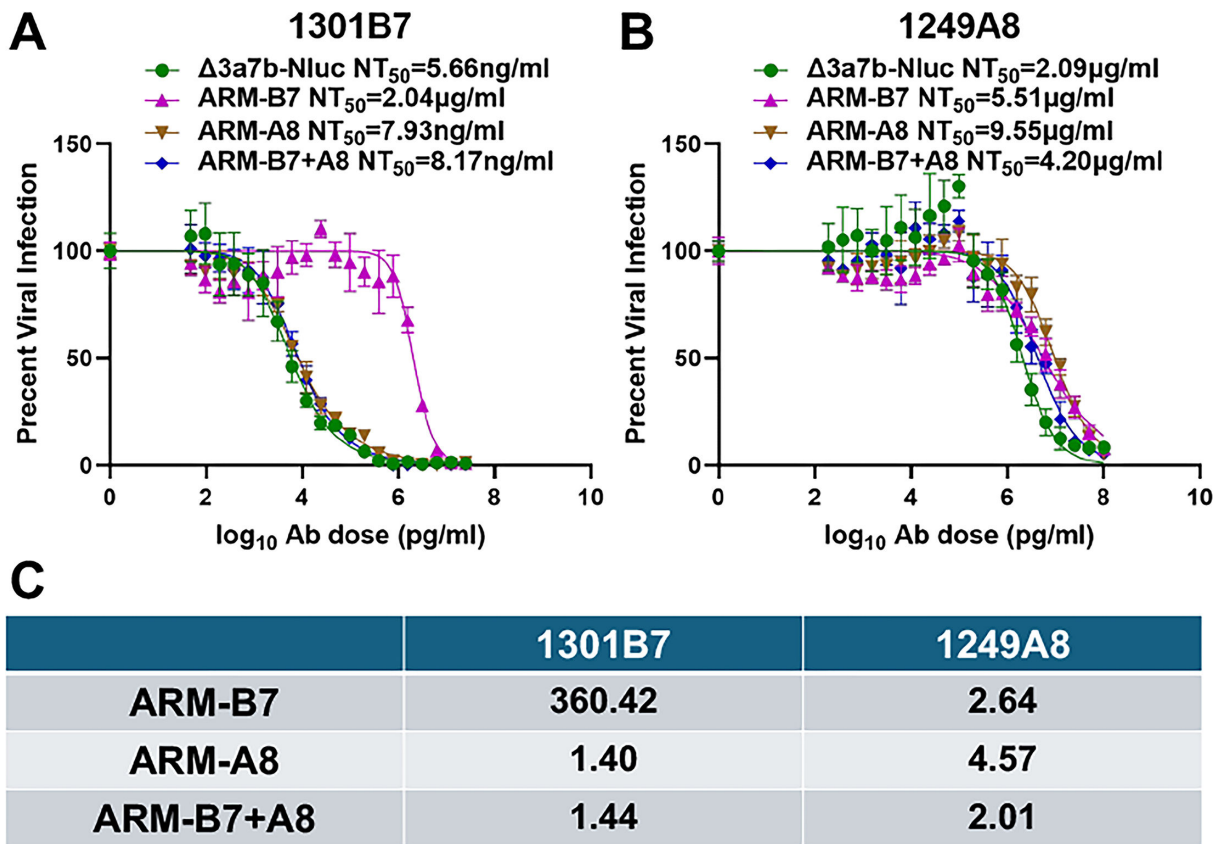


FIG 3 Neutralizing activity of 1301B7 and 1249A8 with parental and ARMs. Plaque reduction neutralization tests (PRNT) were used to assess the sensitivity of the parental virus ($\Delta 3a7b$ -Nluc) and ARM variants (ARM-B7, ARM-A8, ARM-B7 + A8) to NAbs 1301B7 (A) and 1249A8 (B). Neutralization curves were fitted using nonlinear regression (GraphPad Prism) to calculate the half-maximal neutralization titer (NT_{50}). Data are shown as mean \pm SD. The dashed line indicates 50% inhibition. (C) Fold change in NT_{50} for each ARM relative to the parental virus against 1301B7 or 1249A8 NAbs.

sequencing from RT-PCR products and confirmed the presence of these mutations in the S protein of the respective ARMs (Fig. 4B). Structural mapping revealed that S371F in ARM-B7 lies outside the 1301B7 binding sites (Fig. 4C), suggesting an allosteric mechanism of escape rather than a direct disruption of NAb binding. The T299I mutation in ARM-A8, which is also located outside the 1249A8 epitope, conferred only minimal resistance to 1249A8 (less than fivefold).

S371F mutation confers broad-spectrum resistance across RBD epitope classes

We further investigated the functional impact of S371F mutation by testing its effect on a panel of NAbs targeting distinct epitopes on the S1 RBD of SARS-CoV-2 S protein (Fig. 5). Compared to the parental $\Delta 3a7b$ -Nluc ($NT_{50} = 2.84$ ng/mL), ARM-B7 mutant showed a greater than 300-fold increase in resistance to casirivimab ($NT_{50} = 872.97$ ng/mL) (Fig. 5A and D), which targets a Class I epitope. Resistance was even more pronounced against NAb SC27, which targets a cross-reactive class I and IV epitope, with ARM-B7 ($NT_{50} >10$ μ g/mL) showing greater than 679-fold reduction in susceptibility (Fig. 5B and D). Furthermore, the ARM-B7 mutant also exhibited high-level resistance ($NT_{50} >100$ μ g/mL, >307 fold increase) to sotrovimab, a Class III-targeting antibody (Fig. 5C and D). Binding sites of casirivimab (blue) (29), SC27 (yellow) (30), and sotrovimab (red) (31) have been previously described and shown in Fig. 5E. S371 amino acid locates within the SC27 binding site (yellow) and is shown in magenta. This broad, pan-resistance profile indicates that S371F mutation does not merely affect a single epitope but most

Downloaded from https://journals.asm.org/journal/spectrum on 05 May 2026 by 185.72.66.104.

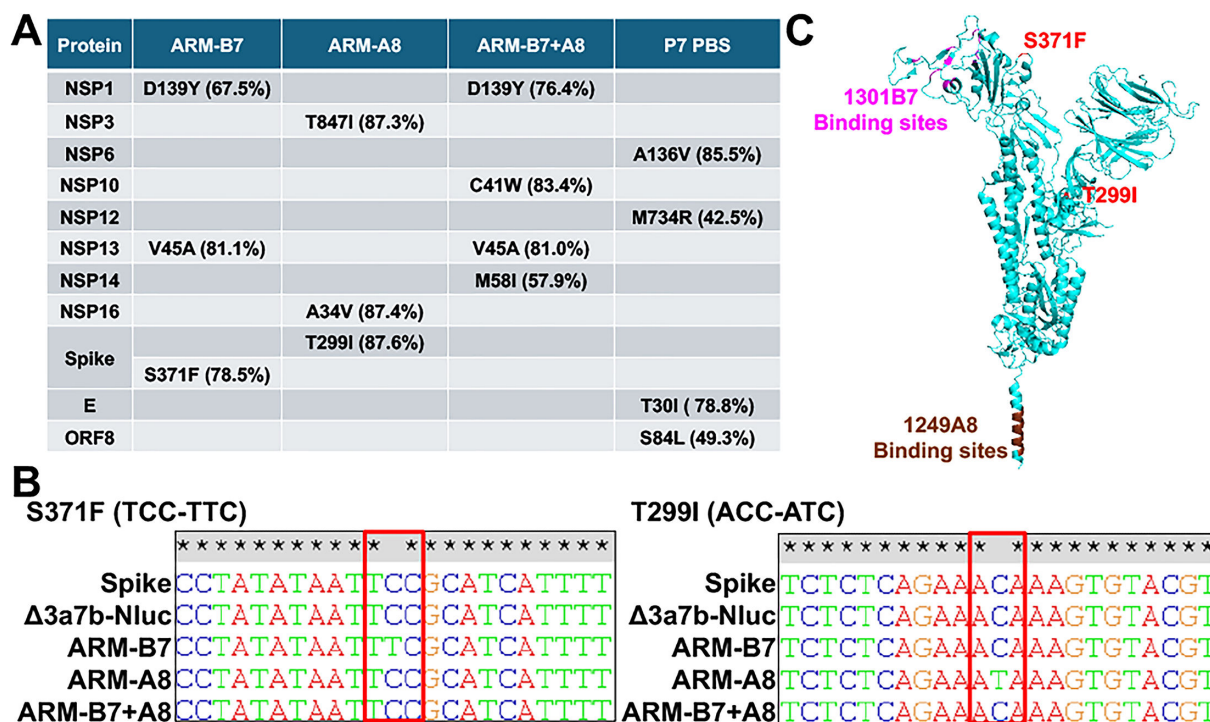


FIG 4 Identification of resistance-conferring mutations in the ARM variants. (A) Amino acid substitutions present at >30% frequency in serially seven times passaged Δ3a7b-Nluc under selective pressure of 1301B7 (ARM-B7), 1249A8 (ARM-A8), their cocktail (ARM-B7 + A8) or PBS (P7 PBS), as identified by NGS. S371F in ARM-B7 and T299I in ARM-A8 within the S protein identified as candidates for conferring resistance. (B) Sanger sequencing chromatograms confirming the presence of the S371F and T299I mutations in the S gene. (C) Structural localization of S371F and T299I mutations (red) within the SARS-CoV-2 S trimer (cyan, PDBID: 6XR8). The binding sites of 1301B7 (magenta) and 1249A8 (brown) are shown.

likely induces a conformational change that compromises the neutralization capacity of antibodies across multiple RBD classes.

DISCUSSION

Therapeutic NAb have represented a critical intervention for the treatment of SARS-CoV-2 infection, yet all FDA-approved NAb therapies have ultimately been rendered ineffective due to viral evolution (11–13). Although S1 RBD-targeting NAb combination therapies demonstrate reduced susceptibility to escape compared to single NAb treatment, they remain vulnerable to the selection of ARMs, even when targeting non-overlapping epitopes due to the S1 RBD’s inherent mutational malleability (32–35). The potent neutralizing capacity of FDA-approved S1 RBD-targeted clinical NAb failure has forced a strategic reassessment of targeted therapeutic options. Our findings provide compelling evidence that NAb targeting the conserved S2 SH in SARS-CoV-2 S protein exhibit superior resistance profiles for the selection of ARMs, and that combining S2 SH- and S1 RBD-targeting NAb creates synergistic pressure for the selection of ARMs, significantly outperforming the use of S1 RBD NAb or RBD NAb-combinations. These results establish a new paradigm for NAb therapeutic development against SARS-CoV-2 that emphasizes targeting conserved epitopes alongside strategic multi-domain combinations, with careful consideration of epitope landscapes to minimize mutations tolerance, thereby informing the design of more durable evasion-resistant NAb therapeutics.

Unlike most screened NAb-resistant mutations that occur directly at or around epitope binding sites (32, 33, 36), the resistance profile of ARM-B7 suggests a distinct mechanism involving antigenic surfaces remodeling of the S protein. This arises from 1301B7’s ability to target relatively conserved regions of the S1 RBD while tolerating for

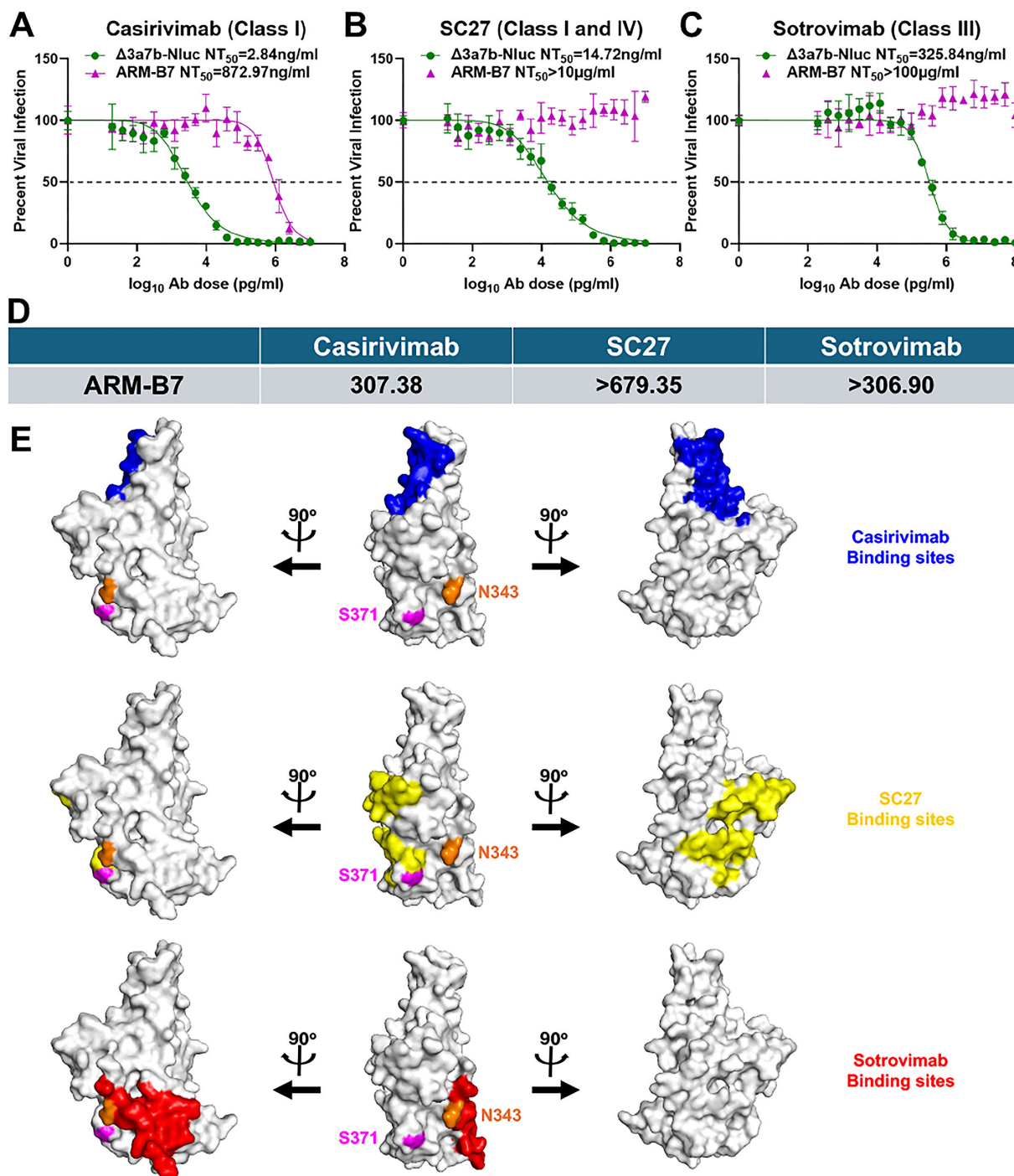


FIG 5 S371F mutation in ARM-B7 confers broad-spectrum resistance to S1 RBD-targeting NABs. Neutralization sensitivity of the parental $\Delta 3a7b$ -Nluc virus and the ARM-B7 escape variant to casirivimab (A), SC27 (B), and sotrovimab (C) was assessed by PRNT in Vero-AT cells. Dose-response curves were fitted by nonlinear regression to calculate NT₅₀ values. Data are shown as mean \pm SD. The dashed line indicates 50% inhibition. (D) Fold change in NT₅₀ of ARM-B7 relative to the parental virus against casirivimab, SC27, and sotrovimab NABs. (E) Binding sites in SARS-CoV-2 Spike RBD (gray, PDBID: 6XDG) for casirivimab (blue), SC27 (yellow), and sotrovimab (red). S371 is located within the SC27 binding site and shown in magenta. N343 is located within the sotrovimab binding site and shown in orange.

others' site diversity, making escape more difficult (16). It has been previously reported that S371F mutation alone affects the neutralizing activity of multiple antibodies targeting all four epitope classes in the SARS-CoV-2 Spike RBD (37, 38). Notably, in the

most recent study (37, 38), the authors demonstrate that mutation S375F rescues the neutralizing activity of antibodies that lost their neutralizing activity with the S371F mutation (37, 38). Importantly, S371F has appeared in all SARS-CoV-2 strains after Omicron BA.2, but it does not occur alone. S373P, S375F, and S376A appeared together with S371F in all SARS-CoV-2 strains after Omicron BA.2. Since S375F has been shown to restore neutralizing activity of antibodies against mutants containing S371F alone (37, 38), we believe that the single mutation S371F identified in our study with ARM-B7 can explain the reduced neutralizing ability of 1301B7, as well as other antibodies targeting different classes of epitope domains in SARS-CoV-2 Spike RBD. However, due to the ability of S375F to restore the neutralizing activity of antibodies, 1301B7 remains effective against Omicron BA.5, XBB.1.5, and JN.1 strains. It is also possible that other mutations (e.g., S373P and S376A) could also play a role in restoring the neutralizing activity of 1301B7 against more recent SARS-CoV-2 Omicron strains. In our study, the single S371F mutation also affected the neutralizing activity of multiple S1 RBD NAb, including casirivimab (Class I) (29), SC27 (classes I and IV) (30), and sotrovimab (Class III) (31), similar to that described in previous studies (37, 38). S371L/F substitution contributes to the reconstruction of an RBD loop, which mediated the tightly packed RBD-RBD interface to help the 3-RBD-down state more stable. This rearranged conformation leads to reduced exposure of the ACE2 receptor binding site (Class I/II epitopes) (37–41). Additionally, the bulky Phe resulting from the S371F substitution induces N343-glycan displacement that hinders Class III antibody binding (Fig. 5E) (38, 42). Furthermore, S371F substitution is involved in the reconstruction of the S371-S373-S375 loop, leading to the elimination of antibody activity that recognizes this epitope (Class IV) (Fig. 5E) (38, 43). S371F exemplifies how single-site changes can reshape SARS-CoV-2 S protein structure to evade all four classes of S1 RBD targeting NAb (38, 44). Overall, S371F mediates immune escape not only through direct epitope disruption but also by inducing structural alterations in S protein that undermine NAb recognition, highlighting the strategic versatility of SARS-CoV-2 in evading humoral immunity.

1249A8 potentially neutralizes SARS-CoV-2 infection by targeting a highly conserved SH epitope within the S2 stem domain of the S protein, effectively disrupting the conformational changes required for membrane fusion (22, 23). By binding on this structurally conserved region, which remains invariant across the vast majority of SARS-CoV-2 variants, 1249A8 disrupts the post-fusion S protein's ability to initiate membrane fusion, thereby blocking viral entry (22). Notably, 1249A8 demonstrates broad cross-neutralization not only against diverse SARS-CoV-2 variants but also across multiple β -coronaviruses, including SARS-CoV and MERS-CoV, underscoring its potential as a pan- β -coronavirus NAb therapeutic candidate (23). Notably, the screening process did not yield any highly potent escape mutants, indicating a high barrier to resistance and supporting the broad therapeutic promise of this NAb. One of the limitations in our study is the lack of additional passages of Δ 3a7b-Nluc in the presence of 1249A8 or 1301B7 + 1249A8. It is possible that additional passage of Δ 3a7b-Nluc in the presence of 1249A8 or 1301B7 + 1249A8 might eventually yield the selection of ARM(s). However, we decided to analyze by NGS and Sanger sequencing all the viruses after the same number of passages (P7). Previous studies have shown that antibody combination therapy can reduce the risk of generating antibody escape mutants (32–35). While our studies suggest that treatment with 1249A8 alone prevents the emergence of antibody-resistant mutants (ARM), its neutralizing potency is weaker compared to 1301B7, favoring the hypothesis that 1249A8 can be used in a combinatory antibody therapy to prevent the emergence of ARM-B7 during monotherapy treatment with 1301B7 alone.

For our studies, we developed a Nluc-expressing attenuated recombinant SARS-CoV-2 (Δ 3a7b-Nluc) incorporating two modifications to facilitate easy identification of antiviral resistance under safe experimental conditions (26). First, the deletion of accessory ORF3a and ORF7b proteins achieves viral attenuation while preserving viral replication. Second, the expression of Nluc enables sensitive and quantitative monitoring of viral propagation and identification of ARMs (25–28). This novel platform effectively addresses

the biosafety constraints inherent in conducting similar experiments using WT SARS-CoV-2 while maintaining bona fide SARS-CoV-2 replication rather than pseudotyped approaches that are essential to accurately identify authentic viral resistant mutants. Importantly, we have previously described that the NT₅₀ of 1301B7 against SARS-CoV-2 WA1 natural strain is 2 ng/mL that reflects that observed in our study with Δ3a7b-Nluc (NT₅₀ 5.66 ng/ml, Fig. 3A) (16). Likewise, the NT₅₀ of 1249A8 against SARS-CoV-2 WA1 natural strain is 0.69 μg/mL, which is comparable to the NT₅₀ with 3a7b-Nluc in our study (2.09 μg/mL; Fig. 3B) (23). Furthermore, this approach is compatible with high-throughput analysis for the identification of ARMs, thereby offering a versatile and safer standard for resistance surveillance and therapeutic development that can also be safely used to identify ARMs from individual or libraries of antibodies and also with sera samples from naturally infected or vaccinated individuals.

In summary, this study establishes the utility of Δ3a7b-Nluc as a safe and effective approach for identifying ARMs circumventing the biosafety limitations associated with using WT SARS-CoV-2. Our results reveal that the conserved S2 SH region presents a low tolerance for mutations compared to S1 RBD and the rationale of designed NAb cocktail therapies targeting both S1 RBD and S2 SH to effectively suppress the emergence of SARS-CoV-2 ARMs commonly observed using S1 RBD-targeting monotherapies or S1 RBD NAb combinations. Altogether, these findings provide critical insights for developing next-generation resistance-evading NAb therapeutics and demonstrate the value of using attenuated viral platforms to safe and effective resistance analysis without potential biosafety concerns.

MATERIALS AND METHODS

Biosafety

In vitro experiments with Δ3a7b-Nluc were performed under Biosafety Level 2+ (BSL-2+) containment laboratories. These studies were reviewed and approved by Texas BioMed's Institutional Biosafety Committee (IBC).

Cells, viruses, and antibodies

Vero cells stably expressing human angiotensin-converting enzyme 2 (hACE2) and transmembrane protease, serine 2 (TMPRSS2) (Vero-AT cells), were acquired from BEI Resources and cultured in Dulbecco's Modified Eagle's Medium (DMEM) supplemented with 10% fetal bovine serum (FBS; VWR), 100 U/mL penicillin-streptomycin (Corning), and 10 μg/mL puromycin (InvivoGen) to maintain selection pressure. The Δ3a7b-Nluc and 1301B7, 1249A8, and SC27 NABs were previously described (16, 23, 26, 30). Casirivimab (REGN10933) and sotrovimab (S309) were bought from MedChemExpress.

Isolation of antibody-resistant mutants (ARMs)

ARMs were selected in three distinct groups: ARM-B7 (resistant to 1301B7), ARM-A8 (resistant to 1249A8), and ARM-B7 + A8 (resistant to 1301B7 + 1249A8). The selection protocol was as follows: confluent Vero-AT cell monolayers in 12-well plates were infected with Δ3a7b-Nluc virus at a dose of 100–200 plaque-forming units (PFU) per well and incubated at 37°C with 5% CO₂ for 1 h. Following viral adsorption, cells were washed with PBS. For ARM-B7 selection, cells were maintained in culture medium containing increasing concentrations of 1301B7 (starting concentration of 0.625 × NT₅₀ = 3.54 ng/mL based on 1301B7 NT₅₀ against Δ3a7b-Nluc of 5.66 ng/mL) in triplicate wells per antibody concentration. For ARM-A8 selection, cells were treated with increasing concentrations of 1249A8 (starting concentration of 0.625 × NT₅₀ = 1.31 μg/mL based on 1249A8 NT₅₀ against Δ3a7b-Nluc of 2.09 μg/mL) in triplicate wells for each concentration. For the ARM-B7 + A8 group, a combination of both antibodies at a starting concentration of 0.625 × NT₅₀ for each of the antibodies (3.54 ng/mL for 1301B7 and 1.31 μg/mL for 1249A8) was also conducted in triplicate wells per antibody condition. After

72 h, supernatants from the highest antibody concentration exhibiting $\geq 50\%$ cytopathic effect (CPE) were harvested, and viral titers were quantified via Nluc activity to initiate subsequent passages. Following seven serial passages under escalating NAb conditions, P7 $\Delta 3a7b$ -Nluc antibody-resistant mutants (ARMs) were collected, amplified in Vero-AT cells, and stored at -80°C for further analysis.

Half-maximal neutralizing antibody titer (NT₅₀)

Plaque reduction neutralization tests (PRNT) were performed by incubating 100–200 PFU/well of virus with serially diluted antibodies for 1 h at 37°C : 1301B7 starting concentration of $25\ \mu\text{g}/\text{mL}$, 1249A8 starting concentration of $100\ \mu\text{g}/\text{mL}$, casirivimab starting concentration of $10\ \mu\text{g}/\text{mL}$, SC27 starting concentration of $10\ \mu\text{g}/\text{mL}$, and sotrovimab starting concentration of $100\ \mu\text{g}/\text{mL}$. Confluent Vero-AT cells in 96-well plates (quadruplicate wells per condition) were then infected with the antibody-virus mixtures and incubated at 37°C under $5\% \text{CO}_2$ for 1 h. Following viral adsorption, the inoculum was replaced with post-infection medium containing 1% Avicel, and cells were further incubated under the same conditions. At 16 h post-infection, cells were fixed with 10% formalin for 24 h, washed with PBS, and permeabilized with 0.5% Triton X-100 for 15 min at room temperature. After additional washing, cells were immunostained using the SARS-CoV N protein-specific cross-reactive monoclonal antibody 1C7C7 ($1\ \mu\text{g}/\text{mL}$), followed by detection with the Vectastain ABC-HRP Kit and DAB Substrate Kit (Vector Laboratories) according to manufacturer protocols. Viral plaques were detected and quantified using a ChemiDoc MP Imaging System.

Plaque assay and immunostaining

Confluent monolayers of Vero-AT cells in six-well plates were infected with 10-fold serial dilutions of the indicated viruses for 1 h at 37°C under $5\% \text{CO}_2$. Following viral adsorption, cells were overlaid with media containing 1% agar and incubated under identical conditions for 72 h. Cells were subsequently fixed overnight with 10% formaldehyde solution, permeabilized with 0.5% Triton X-100 for 15 min at room temperature and subjected to immunostaining with 1C7C7 ($1\ \mu\text{g}/\text{mL}$). Detection was performed with the Vectastain ABC-HRP Kit and DAB Substrate Kit (Vector Laboratories) according to manufacturer specifications. Plates were scanned and imaged using a ChemiDoc MP Imaging System. Wells were stained with crystal violet for additional visualization and imaged with a ChemiDoc MP Imaging System. The titer of the virus was determined by the number of viral plaques at the corresponding dilution.

Sequencing

Viral genome sequences were confirmed by whole-genome sequencing using the MinION platform (Oxford Nanopore Technologies). Briefly, total RNA was extracted from infected Vero-AT cells using TRIzol reagent (Thermo Fisher Scientific) following the manufacturer's recommendations. cDNA was generated using the SuperScript IV Vilo Master Mix (Invitrogen). PCR amplification was performed with the Artic V5.3.2. NCOV-2019 Panel (Integrated DNA Technologies), and sample libraries were prepared with the Native Barcoding Kit 24 V14 (SQK-NBD114.24, Oxford Nanopore Technologies) following the manufacturer's instructions. Sequencing was performed on R10.4.1 flow cells (FLO-MIN114, Oxford Nanopore Technologies) according to the manufacturer's instructions, and reads were analyzed with Geneious Prime software by alignment to the reference sequence. To confirm the presence of the S mutations, the region encoding SARS-CoV-2 S protein was amplified by PCR using the Expand High-Fidelity PCR System (Sigma-Aldrich) from cDNA samples. The resulting amplicons were purified and subjected to Sanger sequencing by Plasmidsaurus Inc.

Statistical analysis

All data represent the means \pm standard deviation (SD) for each group and were analyzed with GraphPad Prism.

ACKNOWLEDGMENTS

We want to thank BEI Resources for providing Vero-AT cells.

This work was supported in part by the NIH/NIAID R01 AI161363 (M.R.W., J.J.K., and L.M.-S.) and by Center for Research on Influenza Pathogenesis and Transmission (CRIPT), a NIAID-funded Center of Excellence for Influenza Research and Response (CEIRR, contract #75N93021C00014), and by NIAID grant U19AI135972 to A.G.-S.

AUTHOR AFFILIATIONS

¹Texas Biomedical Research Institute, San Antonio, Texas, USA

²Department of Medicine, Division of Infectious Diseases, University of Alabama at Birmingham, Birmingham, Alabama, USA

³Center of Scientific Excellence for Influenza Viruses, National Research Centre, Giza, Egypt

⁴Graduate School of Biomedical Sciences, Icahn School of Medicine at Mount Sinai, New York, New York, USA

⁵Department of Microbiology, Icahn School of Medicine at Mount Sinai, New York, New York, USA

⁶Virology Department, Faculty of Veterinary Medicine, Cairo University, Giza, Egypt

⁷Global Health and Emerging Pathogens Institute, Icahn School of Medicine at Mount Sinai, New York, New York, USA

⁸Department of Medicine, Icahn School of Medicine at Mount Sinai, New York, New York, USA

⁹The Tisch Cancer Institute, Icahn School of Medicine at Mount Sinai, New York, New York, USA

¹⁰Department of Pathology, Molecular and Cell-Based Medicine, Icahn School of Medicine at Mount Sinai, New York, New York, USA

¹¹The Icahn Genomics Institute, Icahn School of Medicine at Mount Sina, New York, New York, USA

¹²Department of Microbiology, University of Alabama at Birmingham, Birmingham, Alabama, USA

AUTHOR ORCID*s*

Yao Ma [id http://orcid.org/0000-0003-0815-7910](http://orcid.org/0000-0003-0815-7910)

Chengjin Ye [id http://orcid.org/0000-0002-1934-9494](http://orcid.org/0000-0002-1934-9494)

Adolfo García-Sastre [id http://orcid.org/0000-0002-6551-1827](http://orcid.org/0000-0002-6551-1827)

Mark R. Walter [id http://orcid.org/0000-0003-2163-5550](http://orcid.org/0000-0003-2163-5550)

James J. Kobie [id http://orcid.org/0000-0001-8069-0272](http://orcid.org/0000-0001-8069-0272)

Luis Martinez-Sobrido [id http://orcid.org/0000-0001-7084-0804](http://orcid.org/0000-0001-7084-0804)

ADDITIONAL FILES

The following material is available [online](#).

Supplemental Material

Fig. S1 (Spectrum00006-26-50001.tif). Synergistic neutralizing activity of 1301B7 and 1249A8.

REFERENCES

- Iketani S, Ho DD. 2024. SARS-CoV-2 resistance to monoclonal antibodies and small-molecule drugs. *Cell Chem Biol* 31:632–657. <https://doi.org/10.1016/j.chembiol.2024.03.008>
- Davies NG, Abbott S, Barnard RC, Jarvis CI, Kucharski AJ, Munday JD, Pearson CAB, Russell TW, Tully DC, Washburne AD, Wenseleers T, Gimma A, Waites W, Wong KLM, van Zandvoort K, Silverman JD, Diaz-Ordaz K, Keogh R, Eggo RM, Funk S, Jit M, Atkins KE, Edmunds WJ, CMMID COVID-19 Working Group, COVID-19 Genomics UK (COG-UK) Consortium. 2021. Estimated transmissibility and impact of SARS-CoV-2 lineage B.1.1.7 in England. *Science* 372:eabg3055. <https://doi.org/10.1126/science.eabg3055>
- Wang P, Nair MS, Liu L, Iketani S, Luo Y, Guo Y, Wang M, Yu J, Zhang B, Kwong PD, Graham BS, Mascola JR, Chang JY, Yin MT, Sobieszczyk M, Kyratsos CA, Shapiro M, Merabet M, Bellefquih AM, Nourilil J, Maaroufi A, El Fahime E. 2021. Genome sequences of the delta variant (B.1.617.2) and the kappa variant (B.1.617.1) detected in Morocco. *Microbiol Resour Annu* 10:e0072721. <https://doi.org/10.1128/MRA.00727-21>
- Dejnirattisai W, Shaw RH, Supasa P, Liu C, Stuart AS, Pollard AJ, Liu X, Lambe T, Crook D, Stuart DJ, Mongkolsapaya J, Nguyen-Van-Tam JS, Snape MD, Screaton GR, COVsg C. 2022. Reduced neutralisation of SARS-CoV-2 omicron B.1.1.529 variant by post-immunisation serum. *Lancet* 399:234–236. [https://doi.org/10.1016/S0140-6736\(21\)02844-0](https://doi.org/10.1016/S0140-6736(21)02844-0)
- Baden LR, El Sahly HM, Essink B, Kotloff K, Frey S, Novak R, Diemert D, Spector SA, Roupael N, Creech CB, et al. 2021. Efficacy and safety of the mRNA-1273 SARS-CoV-2 vaccine. *N Engl J Med* 384:403–416. <https://doi.org/10.1056/NEJMoa2035389>
- Chalkias S, Whatley JL, Eder F, Essink B, Khetan S, Bradley P, Brosz A, McGhee N, Tomassini JE, Chen X, Zhao X, Sutherland A, Shen X, Girard B, Edwards DK, Feng J, Zhou H, Walsh S, Montefiori DC, Baden LR, Miller JM, Das R. 2023. Original SARS-CoV-2 monovalent and Omicron BA.4/BA.5 bivalent COVID-19 mRNA vaccines: phase 2/3 trial interim results. *Nat Med* 29:2325–2333. <https://doi.org/10.1038/s41591-023-02517-y>
- Liu X, Ng WH, Zusinaite E, Freitas J, Taylor A, Yerragunta V, Aavula SM, Gorriparthi S, Pongsekar S, Bonda RL, et al. 2024. A single-dose intranasal live-attenuated codon deoptimized vaccine provides broad protection against SARS-CoV-2 and its variants. *Nat Commun* 15:7225. <https://doi.org/10.1038/s41467-024-51535-y>
- Lin DY, Du Y, Xu Y, Paritala S, Donahue M, Maloney P. 2024. Durability of XBB.1.5 vaccines against omicron subvariants. *N Engl J Med* 390:2124–2127. <https://doi.org/10.1056/NEJMc2402779>
- Lu Y, Ao D, He X, Wei X. 2024. The rising SARS-CoV-2 JN.1 variant: evolution, infectivity, immune escape, and response strategies. *MedComm* (2020) 5:e675. <https://doi.org/10.1002/mco2.675>
- Wu MY, Carr EJ, Harvey R, Mears HV, Kjaer S, Townsley H, Hobbs A, Ragno M, Herman LS, Adams L, Gambelin S, Howell M, Beale R, Brown M, Williams B, Gandhi S, Swanton C, Wall EC, Bauer DLV. 2022. WHO's therapeutics and COVID-19 living guideline on mAbs needs to be reassessed. *Lancet* 400:2193–2196. [https://doi.org/10.1016/S0140-6736\(22\)01938-9](https://doi.org/10.1016/S0140-6736(22)01938-9)
- Ai J, Wang X, He X, Zhao X, Zhang Y, Jiang Y, Li M, Cui Y, Chen Y, Qiao R, Li L, Yang L, Li Y, Hu Z, Zhang W, Wang P. 2022. Antibody evasion of SARS-CoV-2 Omicron BA.1, BA.1.1, BA.2, and BA.3 sub-lineages. *Cell Host Microbe* 30:1077–1083. <https://doi.org/10.1016/j.chom.2022.05.001>
- Cao Y, Wang J, Jian F, Xiao T, Song W, Yisimayi A, Huang W, Li Q, Wang P, An R, et al. 2022. Omicron escapes the majority of existing SARS-CoV-2 neutralizing antibodies. *Nature* 602:657–663. <https://doi.org/10.1038/s41586-021-04385-3>
- Yan R, Zhang Y, Li Y, Xia L, Guo Y, Zhou Q. 2020. Structural basis for the recognition of SARS-CoV-2 by full-length human ACE2. *Science* 367:1444–1448. <https://doi.org/10.1126/science.abb2762>
- Wang Q, Zhang Y, Wu L, Niu S, Song C, Zhang Z, Lu G, Qiao C, Hu Y, Yuen KY, Wang Q, Zhou H, Yan J, Qi J. 2020. Structural and functional basis of SARS-CoV-2 entry by using human ACE2. *Cell* 181:894–904. <https://doi.org/10.1016/j.cell.2020.03.045>
- Piepenbrink MS, Khalil AM, Chang A, Mostafa A, Basu M, Sarkar S, Panjiwani S, Ha YH, Ma Y, Ye C, Wang Q, Green TJ, Kizziah JL, Erdmann NB, Goepfert PA, Liu L, Ho DD, Martinez-Sobrido L, Walter MR, Kobie JJ. 2024. Potent neutralization by a RBD antibody with broad specificity for SARS-CoV-2 JN.1 and other variants. *Npj Viruses* 2:55. <https://doi.org/10.1038/s44298-024-00063-z>
- Pinto D, Sauer MM, Czudnochowski N, Low JS, Tortorici MA, Housley MP, Noack J, Walls AC, Bowen JE, Guarino B, et al. 2021. Broad betacoronavirus neutralization by a stem helix-specific human antibody. *Science* 373:1109–1116. <https://doi.org/10.1126/science.abj3321>
- Wang C, van Haperen R, Gutiérrez-Álvarez J, Li W, Okba NMA, Albuelsu I, Widjaja I, van Dieren B, Fernandez-Delgado R, Sola I, Hurdis DL, Daramola O, Grosveld F, van Kuppeveld FJM, Haagmans BL, Enjuanes L, Drabek D, Bosch B-J. 2021. A conserved immunogenic and vulnerable site on the coronavirus spike protein delineated by cross-reactive monoclonal antibodies. *Nat Commun* 12:1715. <https://doi.org/10.1038/s41467-021-21968-w>
- Li T, Kan Q, Ge J, Wan Z, Yuan M, Huang Y, Xie Q, Yang Y, Shao H, Li X, Ye L, Qin A, Bu Z, Liu P, Ye J. 2021. A novel linear and broadly neutralizing peptide in the SARS-CoV-2 S2 protein for universal vaccine development. *Cell Mol Immunol* 18:2563–2565. <https://doi.org/10.1038/s41423-021-00778-6>
- Hsieh C-L, Werner AP, Leist SR, Stevens LJ, Falconer E, Goldsmith JA, Chou C-W, Abiona OM, West A, Westendorf K, Muthuraman K, Fritch EJ, Dinnon KH III, Schäfer A, Denison MR, Chappell JD, Baric RS, Graham BS, Corbett KS, McLellan JS. 2021. Stabilized coronavirus spike stem elicits a broadly protective antibody. *Cell Rep* 37:109929. <https://doi.org/10.1016/j.celrep.2021.109929>
- Ma Y, Wang Y, Dong C, Gonzalez GX, Zhu W, Kim J, Wei L, Kang SM, Wang BZ. 2022. SARS-CoV-2 spike stem protein nanoparticles elicited broad ADCC and robust neutralization against variants in mice. *Small* 18:e2200836. <https://doi.org/10.1002/sml.202200836>
- Deshpande A, Schormann N, Piepenbrink MS, Martinez Sobrido L, Kobie JJ, Walter MR. 2023. Structure and epitope of a neutralizing monoclonal antibody that targets the stem helix of β coronaviruses. *FEBS J* 290:3422–3435. <https://doi.org/10.1111/febs.16777>
- Piepenbrink MS, Park JG, Deshpande A, Loos A, Ye C, Basu M, Sarkar S, Khalil AM, Chauvin D, Woo J, Lovalenti P, Erdmann NB, Goepfert PA, Truong VL, Bowen RA, Walter MR, Martinez-Sobrido L, Kobie JJ. 2022. Potent universal beta-coronavirus therapeutic activity mediated by direct respiratory administration of a Spike S2 domain-specific human neutralizing monoclonal antibody. *PLoS Pathog* 18:e1010691. <https://doi.org/10.1371/journal.ppat.1010691>
- Li CJ, Chang SC. 2023. SARS-CoV-2 spike S2-specific neutralizing antibodies. *Emerg Microbes Infect* 12:220582. <https://doi.org/10.1080/22221751.2023.2220582>
- Ye C, Park J-G, Chiem K, Dravid P, Allué-Guardia A, Garcia-Vilanova A, Pino Tamayo P, Shivanna V, Kapoor A, Walter MR, Kobie JJ, Plemper RK, Torrelles JB, Martinez-Sobrido L. 2023. Immunization with recombinant accessory protein-deficient SARS-CoV-2 protects against lethal challenge and viral transmission. *Microbiol Spectr* 11:e00653-23. <https://doi.org/10.1128/spectrum.00653-23>
- Ma Y, Ye C, Khalil AM, Mahmoud SH, Sobolik EB, Greninger AL, Castro E, Jackson N, Bayoumi M, Plemper RK, Martinez-Sobrido L. 2025. A luminescent attenuated SARS-CoV-2 for the identification and validation of drug-resistant mutants. *J Virol* 99:e00821-25. <https://doi.org/10.1128/jvi.00821-25>
- Hartmann S, Radochonski L, Ye C, Martinez-Sobrido L, Chen J. 2025. SARS-CoV-2 ORF3a drives dynamic dense body formation for optimal viral infectivity. *Nat Commun* 16:4393. <https://doi.org/10.1038/s41467-025-59475-x>
- Silvas JA, Vasquez DM, Park J-G, Chiem K, Allué-Guardia A, Garcia-Vilanova A, Platt RN, Miorin L, Kehrer T, Cupic A, Gonzalez-Reiche AS, Bakel H van, García-Sastre A, Anderson T, Torrelles JB, Ye C, Martinez-Sobrido L. 2021. Contribution of SARS-CoV-2 accessory proteins to viral pathogenicity in K18 human ACE2 transgenic mice. *J Virol* 95:e0040221. <https://doi.org/10.1128/JVI.00402-21>
- Hansen J, Baum A, Pascal KE, Russo V, Giordano S, Wloga E, Fulton BO, Yan Y, Koon K, Patel K, et al. 2020. Studies in humanized mice and convalescent humans yield a SARS-CoV-2 antibody cocktail. *Science* 369:1010–1014. <https://doi.org/10.1126/science.abb0827>
- Voss WN, Mallory ML, Byrne PO, Marchioni JM, Knudson SA, Powers JM, Leist SR, Dadonaite B, Townsend DR, Kain J, Huang Y, Satterwhite E, Castillo IN, Mattocks M, Paresi C, Munt JE, Scobey T, Seeger A, Premkumar L, Bloom JD, Georgiou G, McLellan JS, Baric RS, Lavinder JJ,

- Ippolito GC. 2024. Hybrid immunity to SARS-CoV-2 arises from serological recall of IgG antibodies distinctly imprinted by infection or vaccination. *Cell Reports Medicine* 5:101668. <https://doi.org/10.1016/j.xcr.2024.101668>
31. Pinto D, Park Y-J, Beltramello M, Walls AC, Tortorici MA, Bianchi S, Jaconi S, Culap K, Zatta F, De Marco A, Peter A, Guarino B, Spreafico R, Cameroni E, Case JB, Chen RE, Havenar-Daughton C, Snell G, Telenti A, Virgin HW, Lanzavecchia A, Diamond MS, Fink K, Veelsler D, Corti D. 2020. Cross-neutralization of SARS-CoV-2 by a human monoclonal SARS-CoV antibody. *Nature* 583:290–295. <https://doi.org/10.1038/s41586-020-2349-y>
 32. Baum A, Fulton BO, Wloga E, Copin R, Pascal KE, Russo V, Giordano S, Lanza K, Negron N, Ni M, Wei Y, Atwal GS, Murphy AJ, Stahl N, Yancopoulos GD, Kyrtatsous CA. 2020. Antibody cocktail to SARS-CoV-2 spike protein prevents rapid mutational escape seen with individual antibodies. *Science* 369:1014–1018. <https://doi.org/10.1126/science.abd0831>
 33. Copin R, Baum A, Wloga E, Pascal KE, Giordano S, Fulton BO, Zhou A, Negron N, Lanza K, Chan N, et al. 2021. The monoclonal antibody combination REGEN-COV protects against SARS-CoV-2 mutational escape in preclinical and human studies. *Cell* 184:3949–3961. <https://doi.org/10.1016/j.cell.2021.06.002>
 34. Cox M, Peacock TP, Harvey WT, Hughes J, Wright DW, Consortium C-G, Willett BJ, Thomson E, Gupta RK, Peacock SJ, Robertson DL, Carabelli AM. 2023. SARS-CoV-2 variant evasion of monoclonal antibodies based on *in vitro* studies. *Nat Rev Microbiol* 21:112–124. <https://doi.org/10.1038/s41579-022-00809-7>
 35. Ragonnet-Cronin M, Nutalai R, Huo J, Djokaite-Guraliuc A, Das R, Tuekprakhon A, Supasa P, Liu C, Selvaraj M, Groves N, et al. 2023. Generation of SARS-CoV-2 escape mutations by monoclonal antibody therapy. *Nat Commun* 14:3334. <https://doi.org/10.1038/s41467-023-37826-w>
 36. Gupta A, Konnova A, Smet M, Berkell M, Savoldi A, Morra M, Van Averbeke V, De Winter FH, Peserico D, Danese E, Hotterbeekx A, Righi E, mAb ORCHESTRA working group, De Nardo P, Tacconelli E, Malhotra-Kumar S, Kumar-Singh S. 2023. Host immunological responses facilitate development of SARS-CoV-2 mutations in patients receiving monoclonal antibody treatments. *J Clin Invest* 133:e166032. <https://doi.org/10.1172/JCI166032>
 37. Liu S, Liu P, Lu Q, Shen Y, Zhang L, Liang Z, Yu Y, Huang W, Wang Y. 2025. The compensatory effect of S375F on S371F is vital for maintaining the infectivity of SARS - CoV - 2 omicron variants. *J Med Virol* 97:e70242. <https://doi.org/10.1002/jmv.70242>
 38. Liu L, Iketani S, Guo Y, Chan JF-W, Wang M, Liu L, Luo Y, Chu H, Huang Y, Nair MS, Yu J, Chik KK-H, Yuen TT-T, Yoon C, To KK-W, Chen H, Yin MT, Sobieszczyk ME, Huang Y, Wang HH, Sheng Z, Yuen K-Y, Ho DD. 2022. Striking antibody evasion manifested by the Omicron variant of SARS-CoV-2. *Nature* 602:676–681. <https://doi.org/10.1038/s41586-021-04388-0>
 39. Dejnirattisai W, Huo J, Zhou D, Zahradnik J, Supasa P, Liu C, Duyvesteyn HME, Ginn HM, Mentzer AJ, Tuekprakhon A, et al. 2022. SARS-CoV-2 Omicron-B.1.1.529 leads to widespread escape from neutralizing antibody responses. *Cell* 185:467–484. <https://doi.org/10.1016/j.cell.2021.12.046>
 40. Miller NL, Clark T, Raman R, Sasisekharan R. 2022. A structural dynamic explanation for observed escape of SARS-CoV-2 BA.2 variant mutation S371L/F. *bioRxiv*:2022.02.25.481957. <https://doi.org/10.1101/2022.02.25.481957>
 41. Gobeil SM-C, Henderson R, Stalls V, Janowska K, Huang X, May A, Speakman M, Beaudoin E, Manne K, Li D, Parks R, Barr M, Deyton M, Martin M, Mansouri K, Edwards RJ, Eaton A, Montefiori DC, Sempowski GD, Saunders KO, Wiehe K, Williams W, Korber B, Haynes BF, Acharya P. 2022. Structural diversity of the SARS-CoV-2 Omicron spike. *Mol Cell* 82:2050–2068. <https://doi.org/10.1016/j.molcel.2022.03.028>
 42. Cao Y, Yisimayi A, Jian F, Xiao T, Song W, Wang J, Du S, Zhang Z, Liu P, Hao X, et al. 2022. Omicron BA.2 specifically evades broad sarbecovirus neutralizing antibodies. *bioRxiv*. <https://doi.org/10.1101/2022.02.07.479349>
 43. Stalls V, Lindenberger J, Gobeil SM-C, Henderson R, Parks R, Barr M, Deyton M, Martin M, Janowska K, Huang X, May A, Speakman M, Beaudoin E, Kraft B, Lu X, Edwards RJ, Eaton A, Montefiori DC, Williams WB, Saunders KO, Wiehe K, Haynes BF, Acharya P. 2022. Cryo-EM structures of SARS-CoV-2 Omicron BA.2 spike. *Cell Rep* 39:111009. <https://doi.org/10.1016/j.celrep.2022.111009>
 44. Iketani S, Liu L, Guo Y, Liu L, Chan JF-W, Huang Y, Wang M, Luo Y, Yu J, Chu H, Chik KK-H, Yuen TT-T, Yin MT, Sobieszczyk ME, Huang Y, Yuen K-Y, Wang HH, Sheng Z, Ho DD. 2022. Antibody evasion properties of SARS-CoV-2 Omicron sublineages. *Nature* 604:553–556. <https://doi.org/10.1038/s41586-022-04594-4>